Inorg. Chem. **2002**, *41*, 1478–1491

Synthesis, Structure, and Magnetic Properties of Tetranuclear Cubane-like and Chain-like Iron(II) Complexes Based on the N_4O Pentadentate Dinucleating Ligand 1,5-Bis[(2-pyridylmethyl)amino]pentan-3-ol

Juan M. Clemente-Juan,[†] Christine Mackiewicz,[†] Marc Verelst,[†,‡] Françoise Dahan,[†] Azzedine Bousseksou,[†] Yiannis Sanakis,[§,||] and Jean-Pierre Tuchagues*[,†]

Laboratoire de Chimie de Coordination, UPR CNRS 8241, 205 route de Narbonne, 31077 Toulouse, France, Institute of Materials Science, NCSR "Demokritos", 15310 Aghia Paraskevi, Athens, Greece, and Department of Biological Applications and Technologies, University of Ioannina, 45110 Ioannina, Greece

Received July 24, 2001

The tetranuclear complexes $[Fe_4(pypentO)(pym)_3(Oac)(NCS)_3]\cdot 1.5EtOH$ (**1**), $[Fe_4(pypentO)(pym)(Oac)_2(NCS)_2(MeO)_2(H_2O)]\cdot H_2O$ (**2**), $[Fe_2(pypentO)(NCO)_3]_2$ (**3**), and $[Fe_2(pypentO)(N_3)_3]_2$ (**4**) have been prepared, and their structure and magnetic properties have been studied (pypentOH = 1,5-bis[(2-pyridylmethyl)amino]pentan-3-ol, pymH = 2-pyridylmethanol). The X-ray diffraction analysis of **1** ($C_{43}H_{53}N_{10}O_{7.5}S_3Fe_4$, monoclinic, $P2_1/n$, $a = 11.6153(17)$ Å, $b = 34.391(17)$ Å, $c = 14.2150(18)$ Å, $\beta = 110.88(5)°$, $V = 5305(3)$ Å^3, $Z = 4$) and **2** ($C_{31}H_{45}N_7O_{10}S_2Fe_4$, monoclinic, $C2/c$, $a = 19.9165(17)$ Å, $b = 21.1001(12)$ Å, $c = 21.2617(19)$ Å, $\beta = 104.441(10)°$, $V = 8652.7(12)$ Å^3, $Z = 8$) showed a Fe_4O_4 cubane-like arrangement of four iron(II) atoms, four μ_3-O bridging ligands, one (**1**) or two (**2**) syn–syn bridging acetates. The X-ray diffraction analysis of **3** ($C_{40}H_{46}N_{14}O_8Fe_4$, monoclinic, $P2_1/c$, $a = 11.7633(18)$ Å, $b = 18.234(3)$ Å, $c = 10.4792(16)$ Å, $\beta = 99.359(18)°$, $V = 2217.7(6)$ Å^3, $Z = 2$) and **4** ($C_{34}H_{46}N_{26}O_2Fe_4$, monoclinic, $P2_1/c$, $V = 4412.4(10)$ Å^3, $a = 23.534(3)$ Å, $b = 18.046(2)$ Å, $c = 10.4865(16)$ Å, $\beta = 97.80(2)°$, $Z = 4$) showed a zigzag bis-dinuclear arrangement of four iron(II) cations, two μ_2-O bridging pypentO ligands, four μ_2-N-cyanato bridging ligands (**3**) or four end-on azido bridging ligands (**4**): they are the first examples of cyanato and azido bridged discrete polynuclear ferrous compounds, respectively. The Mössbauer spectra of **1** are consistent with four different high-spin iron(II) sites in the Fe_4O_4 cubane-type structure. The Mössbauer spectra of **3** are consistent with two high-spin iron(II) sites (N_5O and N_4O). Below 190 K, the Mössbauer spectra of **4** are consistent with one N_5O and two N_4O high-spin iron(II) sites. The temperature dependence of the magnetic susceptibility was fitted with $J_1 \sim 0$ cm^{-1}, $J_2 = -1.3$ cm^{-1}, $J_3 = 4.6$ cm^{-1}, $D = 6.4$ cm^{-1}, and $g = 2.21$ for **1**; $J_1 = 2.6$ cm^{-1}, $J_2 = 2.5$ cm^{-1}, $J_3 = -5.6$ cm^{-1}, $D = 4.5$ cm^{-1}, and $g = 2.09$ for **2**; $J_1 = 1.5$ cm^{-1}, $J_2 = 0.2$ cm^{-1}, $D = -5.6$ cm^{-1}, $D' = 4.5$ cm^{-1}, and $g = 2.14$ for **3**; and $J_1 = -2.6$ cm^{-1}, $J_2 = 0.8$ cm^{-1}, $D = 6.3$ cm^{-1}, $D' = 1.6$ cm^{-1}, and $g = 2.18$ for **4**. The differences in sign among the J_1, J_2, and J_3 super-exchange interactions indicate that the faces including only μ_3-OR bridges exhibit ferromagnetic interactions. The nature of the ground state in **1**–**3** is confirmed by simulation of the magnetization curves at 2 and 5 K. In the bis-dinuclear iron(II) compounds **3** and **4**, the J_2 interaction resulting from the bridging of two $Fe_2(pypentO)X_3$ units through two pseudo-halide anions is ferromagnetic in **3** (X = μ_2-N-cyanato) and may be either ferro- or antiferromagnetic in **4** (X = end-on azido). The J_1 interaction through the central O_{alkoxo} and pseudo-halide bridges inside the dinuclear units is ferromagnetic in **3** (X = μ_2-N-cyanato) and antiferromagnetic in **4** (X = end-on azido). In agreement with the symmetry of the two Fe^{II} sites in complexes **3** and **4**, D (pentacoordinated sites) is larger than D' (octahedral sites).

10.1021/ic010787+ CCC: $22.00

Published on Web 02/20/2002

Introduction

Significant developments in the chemistry of oxygen-bridged polynuclear iron complexes initially resulted from discovery of the biological role of oxygen-bridged poly-iron centers.[1] Synthetic efforts to prepare model complexes of iron proteins has yielded several unexpected and interesting oxygen-bridged poly-iron compounds, the magnetic properties of which have motivated interesting studies concerning their unusual electronic structure.[2] Recognition of the interest of such poly-iron compounds as building blocks for molecular-based magnetic materials then became the major incentive for further developments in their chemistry.[3] With the exception of dinuclear compounds, discrete poly-iron molecules exclusively involve either oxygen or sulfur bridges, while cyanato, thiocyanato, azido, etc. bridges are common in discrete polynuclear species involving other transition metal ions.[4] Apart from the iron−sulfur clusters, the numerous tetranuclear iron species reported in the literature include most frequently μ-oxo bridges associated with other O-bridging moieties (hydroxo, carboxylato, carbonato, alkoxo, phenoxo, etc.) in Fe^{III}_4 compounds, yielding a variety of geometries for the Fe_4 array: butterfly,[5] square or rectangular planar,[6] tetrahedral,[7] and puckered $(-Fe-O-)_4$ ring.[8] The few reported exceptions to the presence of μ-oxo bridges in Fe^{III}_4 compounds include the following Fe_4 arrays (O-bridging moieties): adamantanoid (bis-diketonato),[9] triangular with central iron (alkoxo),[10] defective double cubane (alkoxo),[11] and distorted tetrahedral (oximato).[12] Three mixed-valence Fe_4 compounds have been reported, including a cubane array with alkoxo and carboxylato bridges,[13] an adamantanoid array with bis-diketonato bridges,[14] and a rectangular planar array with alkoxo and fluoro bridges.[15] The six Fe^{II}_4 compounds reported include cubane arrays with alkoxo or phenoxo bridges,[13,16] a triangular (+ central iron) array with carboxylato bridges,[17] tetrahedral arrays with one oxo and formamidinato[18] or dipyridilamine[19] bridges, and a linear array with catecholato bridges.[20] Examination of the literature referenced above on tetranuclear iron species shows that the geometry of the Fe_4 array, and the oxidation state of the metal centers, may be controlled by using selected ligands with or without bridging oxygen atoms. Our goal is to explore the possibility of extending poly-iron chemistry in a controlled fashion, i.e., by using dinucleating ligands selected for obtaining coordinatively deficient ferrous species prone to bind pseudo-halide anions as bridging ligands concurrently to oxygen bridges. Actually, pseudo-halide ligands bridging anisotropic ferrous ions in a controlled manner would delineate a new class of discrete poly-iron species that may possess interesting magnetic properties. In this contribution, we describe the first results obtained along this line: the preparation, characterization, X-ray crystal structure, and magnetic study of the cubane-like tetranuclear ferrous complexes $[Fe_4(pypentO)(pym)_3(Oac)(NCS)_3]\cdot 1.5EtOH$ (**1**) and $[Fe_4(pypentO)(pym)(Oac)_2(NCS)_2(MeO)_2(H_2O)]\cdot H_2O$

* Author to whom correspondence should be addressed. E-mail: tuchague@lcctoul.lcc-toulouse.fr.

† Laboratoire de Chimie de Coordination.

‡ Present address: Centre d'Elaboration de Matériaux et d'Etudes Structurales, UPR CNRS 8011, 29 rue Jeanne Marvig, 31055 Toulouse Cédex, France.

§ Institute of Materials Science.

|| University of Ioannina.

(1) Lippard, S. J. *Angew. Chem., Int. Ed. Engl.* **1988**, *27*, 344.

(2) For examples, see: (a) McCusker, J. K.; Christmas, C. A.; Hagen, P. M.; Chadha, R. K.; Harvey, D. F.; Hendrickson, D. N. *J. Am. Chem. Soc.* **1991**, *113*, 6114. (b) Delfs, C.; Gatteschi, D.; Pardi, L.; Sessoli, R.; Wieghardt, K.; Hanke, D. *Inorg. Chem.* **1993**, *32*, 3099.

(3) For example, see: Gatteschi, D.; Sessoli, R.; Cornia, A. *J. Chem. Soc., Chem. Commun.* **2000**, 725.

(4) For example, see: Ribas, J.; Escuer, A.; Monfort, M.; Vicente, R.; Cortés, R.; Lezama, L.; Rojo, T. *Coord. Chem. Rev.* **1999**, *193*−*195*, 1027.

(5) (a) Ponomarev, V. I.; Atovmyan, L. O.; Bobkova, S. A.; Turté, K. I. *Dokl. Akad. Nauk. SSSR.* **1984**, *274*, 368. (b) Armstrong, W. H.; Roth, M. E.; Lippard, S. J. *J. Am. Chem. Soc.* **1987**, *109*, 6318. (c) McCusker, J. K.; Vincent, J. B.; Schmitt, E. A.; Mino, M. L.; Shin, K.; Coggin, D. K.; Hagen, P. M.; Huffman, J. C.; Christou, G.; Hendrickson, D. N. *J. Am. Chem. Soc.* **1991**, *113*, 3012. (d) Wu, L.; Pressprich, M.; Coppens, P.; DeMarco, M. J. *Acta Crystallogr., Sect. C* **1993**, 1255. (e) Chaudhuri, P.; Winter, M.; Freischhauer, P.; Haase, W.; Flörke, U.; Haupt, H.-J. *Inorg. Chim. Acta* **1993**, *212*, 241. (f) Wemple, M. W.; Coggin, D. K.; Vincent, J. B.; McCusker, J. K.; Streib, W. E.; Huffman, J. C.; Hendrickson, D. N.; Christou, G. *J. Chem. Soc., Dalton Trans.* **1998**, 719.

(6) (a) Toftlund, H.; Murray, K. S.; Zwack, P. R.; Taylor, L. F.; Anderson, O. P. *J. Chem. Soc., Chem. Commun.* **1986**, 191. (b) Jameson, D. L.; Xie, C.-L.; Hendrickson, D. N.; Potenza, J. A.; Schugar, H. J. *J. Am. Chem. Soc.* **1987**, *109*, 740. (c) Chen, Q.; Lynch, J. B.; Gomez-Romero, P.; Ben-Hussein, A.; Jameson, G. B.; O'Connor, C. J.; Que, L., Jr. *Inorg. Chem.* **1988**, *27*, 2673. (d) Sessler, J. L.; Sibert, J. W.; Lynch, V.; Markert, J. T.; Wooten, C. L. *Inorg. Chem.* **1993**, *32*, 621. (e) Arulsamy, N.; Glerup, J.; Hodgson, D. J. *Inorg. Chem.* **1994**, *33*, 3043. (f) Yano, S.; Inagaki, T.; Yamada, Y.; Kato, M.; Yamasaki, M.; Sakai, K.; Tsubomura, T.; Sato, M.; Mori, W.; Yamaguchi, K.; Kinoshita, I. *Chem. Lett.* **1996**, 61. (g) Jensen, K. B.; McKenzie, C. J.; Simonsen, O.; Toftlund, H.; Hazell, A. *Inorg. Chim. Acta* **1997**, *257*, 163. (h) Tanase, T.; Inagaki, T.; Yamada, Y.; Kato, M.; Ota, E.; Yamazaki, M.; Sato, M.; Mori, W.; Yamaguchi, K.; Mikuriya, M.; Takahashi, M.; Takeda, M.; Kinoshita, I.; Yano, S. *J. Chem. Soc., Dalton Trans.* **1998**, 713. (i) Trukhan, V. M.; Pierpont, C. G.; Jensen, K. B.; Nordlander, E.; Shteinman, A. A. *J. Chem. Soc., Chem. Commun.* **1999**, 1193. (j) Tanase, T.; Inoue, C.; Ota, E.; Yano, S.; Takahashi, M.; Takeda, M. *Inorg. Chim. Acta* **2000**, *297*, 18. (k) Fernandes, C.; Neves, A.; Vencato, I.; Bortoluzzi, A. J.; Drago, V.; Weyhermuller, T.; Rentschler, E. *Chem. Lett.* **2000**, 540.

(7) (a) Murch, B. P.; Boyle, P. D.; Que, L., Jr. *J. Am. Chem. Soc.* **1985**, *107*, 6728. (b) Murch, B. P.; Bradley, F. C.; Boyle, P. D.; Papafthymiou, V.; Que, L., Jr. *J. Am. Chem. Soc.* **1987**, *109*, 7993. (c) Ye, B.-H.; Li, X.-Y.; Xue, F.; Mak, T. C. W. *J. Chem. Soc., Chem. Commun.* **1997**, 2407.

(8) Cotton, F. A.; Daniels, L. M.; Maloney, D. J.; Murillo, C. A, *Inorg. Chim. Acta* **1996**, *252*, 293.

(9) Saalfrank, R. W.; Hörner, B.; Stalke, D.; Salbeck, J. *Angew. Chem., Int. Ed. Engl.* **1993**, *32*, 1179.

(10) Barra, A. L.; Caneschi, A.; Cornia, A.; de Biani, F.; Fabrizi; Gatteschi, D.; Sangregorio, C.; Sessoli, R.; Sorace, L. *J. Am. Chem. Soc.* **1999**, *121*, 5302.

(11) Li, H.; Zhong, Z. J.; Chen, W.; You, X.-Z. *J. Chem. Soc., Dalton Trans.* **1997**, 463.

(12) Thorpe, J. M.; Beddoes, R. L.; Collison, D.; Garner, C. D.; Helliwell, M.; Holmes, J. M.; Tasker, P. A. A*ngew. Chem., Int. Ed. Engl.* **1999**, *38*, 1119.

(13) Taft, K. L.; Caneschi, A.; Pence, L. E.; Delfs, C. D.; Papaefthymiou, G. C.; Lippard, S. J. *J. Am. Chem. Soc.* **1993**, *115*, 11753.

(14) Saalfrank, R. W.; Burak, R.; Breit, A.; Stalke, D.; Herbst-Irmer, R.; Daub, J.; Porsch, M.; Bill, E.; Müther, M.; Trautwein, A. X. *Angew. Chem., Int. Ed. Engl.* **1994**, *33*, 1621.

(15) Sugimoto, H.; Hayashi, Y.; Koshi, C.; Fujinami, S.; Suzuki, M.; Maeda, Y.; Uehara, A. *Chem. Lett.* **1996**, 933.

(16) Shoner, S. C.; Power, P. P. *Inorg. Chem.* **1992**, *31*, 1001.

(17) (a) Ménage, S.; Fujii, H.; Hendrich, M. P.; Que, L., Jr. *Angew. Chem., Int. Ed. Engl.* **1994**, *33*, 1660. (b) Mandal, S. K.; Young, V. G., Jr.; Que, L., Jr. *Inorg. Chem.* **2000**, *39*, 1831.

(18) Cotton, F. A.; Daniels, L. M.; Falvello, L. R.; Matonic, J. H.; Murillo, C. A.; Wang, X.; Zhou, H. *Inorg. Chim. Acta* **1997**, *266*, 91.

(19) Cotton, F. A.; Daniels, L. M.; Jordan, G. T.; Murillo, C. A.; Pascual, I. *Inorg. Chim. Acta* **2000**, *297*, 6.

(20) Reynolds, R. A., III; Coucouvanis, D. *Inorg. Chem.* **1998**, *37*, 170.

(**2**) and zigzag bis-dinuclear ferrous complexes $[Fe_2(pypentO)(NCO)_3]_2$ (**3**) and $[Fe_2(pypentO)(N_3)_3]_2$ (**4**). The ligands pypentO and pym are the deprotonated forms of 1,5-bis[(2-pyridylmethyl)amino]pentan-3-ol and 2-pyridylmethanol, respectively.

Experimental Section

Materials. 3-Chloropropionyl chloride, sodium borohydride, 2-pyridinecarboxaldehyde, potassium cyanate (Aldrich), aluminum trichloride, potassium phthalimide, potassium thiocyanate, and sodium azide (Fluka) were used as purchased. High-grade solvents used for the synthesis of complexes were distilled prior to use. Iron(II) acetate dihydrate was synthesized as previously described.[21]

Ligand. 1,5-Diaminopentan-3-ol dihydrochloride was synthesized according to a reported method.[22] The free 1,5-diaminopentan-3-ol was obtained by reacting the hydrochloride salt with the stoichiometric amount of freshly prepared sodium ethoxide in ethanol. The Schiff base condensation of 1,5-diaminopentan-3-ol (1 mmol) with 2-pyridinecarboxaldehyde (2 mmol) was carried out in ethanol (10 mL). The reaction mixture was stirred overnight, and the resulting Schiff base (orange solution) was reduced with 2 equiv of solid $NaBH_4$. The reaction mixture was warmed (60 °C) for 2 h and cooled to room temperature, and the salts were eliminated by filtration. The pypentOH ligand was used without further purification.

Complexes. All complexation reactions and sample preparations for physical measurements were carried out in a purified nitrogen atmosphere within a glovebox (Vacuum Atmospheres H.E.43.2) equipped with a dry train (Jahan EVAC 7).

General Procedure. A solution of $Fe(O_2CMe)_2 \cdot 2H_2O$ (420 mg, 2.0 mmol) in EtOH (10 mL) was slowly added to a pypentOH ethanolic solution (1.0 mmol in 10 mL). The dark brown reaction mixture was stirred for a few minutes after which a solution of pseudo-halide salt (3.0 mmol) in 1:1 MeOH/H_2O (5 mL) was added (**1**, **2**: KSCN, 629 mg; **3**: KOCN, 243 mg; **4**: NaN_3, 195 mg), and the mixture was stirred for an additional 15 min and filtrated. The resulting filtrate was allowed to stand for a few days during which brown-orange single crystals were obtained. The only difference in the synthesis of complex **2** with respect to the general procedure described above is the solvent used for preparing the KSCN solution: in the case of **2**, pure MeOH was used instead of the 1:1 MeOH/H_2O mixture.

$[Fe_4(pypentO)(pym)_3(Oac)(NCS)_3]\cdot 1.5EtOH$ (1). Yield: 121 mg, 11.3%. Anal. Calcd (found) for $C_{43}H_{53}N_{10}O_{7.5}S_3Fe_4$: C, 44.93 (44.59); H, 4.65 (4.55); N, 12.18 (11.79); S, 8.37 (8.58); Fe, 19.45 (19.05). Characteristic IR absorptions (KBr): 2061, 2053 ($\nu_{C=N}$), 1561, 1412 ($\nu_{COO}-$), 876 ($\nu_{C=S}$).

$[Fe_4(pypentO)(pym)(Oac)_2(NCS)_2(MeO)_2(H_2O)]\cdot H_2O$ (2). Yield: 103 mg, 10.7%. Anal. Calcd (found) for $C_{31}H_{45}N_7O_{10}S_2Fe_4$: C, 38.66 (38.89); H, 4.71 (4.37); N, 10.18 (10.07); Fe, 23.19 (22.41). Characteristic IR absorptions (KBr): 2049, 2053 ($\nu_{C=N}$), 1570, 1410 ($\nu_{COO}-$), 870 ($\nu_{C=S}$).

$[Fe_2(pypentO)(NCO)_3]_2$ (3). Yield: 135 mg, 14.1%. Anal. Calcd (found) for $C_{40}H_{46}N_{14}O_8Fe_4$: C, 44.72 (44.10); H, 4.32 (4.06); N, 18.25 (17.81); Fe, 20.79 (20.19). Characteristic IR absorptions (KBr): 2205, 2168 ($\nu_{C=N}$), 1348 ($\nu_{C=O}$), 623 (δ_{OCN}).

$[Fe_2(pypentO)(N_3)_3]_2$ (4). Yield: 140 mg, 13.1%. Anal. Calcd (found) for $C_{34}H_{46}N_{26}O_2Fe_4$: C, 38.01 (38.36); H, 4.32 (3.72); N, 33.90 (32.88); Fe, 20.79 (20.34). Characteristic IR absorptions (KBr): 2076, 2051 ($\nu_{N=N}$), 1334 ($\nu_{N=N}$), 641 (δ_{NNN}).

Crystallographic Data Collection and Structure Determination. The selected crystal was pasted on a glass fiber and mounted on a CAD4 Enraf-Nonius diffractometer (**1**) or a Stoe Imaging Plate Diffraction System (IPDS) using graphite-monochromated Mo Kα radiation, and equipped with an oxford cryostream cooler device (**2**−**4**). The data were collected at 293 (**1**), 180 (**2**) and 160 K (**3**, **4**). Final unit cell parameters were obtained by least-squares refinement of the setting angles of 25 reflections with $10.0° < \theta < 15.0°$ for **1** and of a set of 5000 reflections ($I > 10\sigma(I)$ for **2**−**4**. The crystal decay was monitored by measuring three standard reflections every 2 h (**1**) and 200 reflections per image (**2**−**4**). No significant fluctuations of diffracted intensities were observed during the measurements. A total of 7775 (**1**), 27944 (**2**), 17070 (**3**), and 31593 (**4**) reflections were collected. In the refinements were used 7361 unique reflections ($R_{av} = 0.0550$ on I) (**1**) and 6909 (**2**), 4335 (**3**), and 6740 (**4**) independent reflections ($R_{int} = 0.0515$ (**2**), 0.0595 (**3**), 0.0368 (**4**)).

The structures were solved by direct methods using the SHELXS-97[23] program and refined by least-squares procedures on F_o^2 with the SHELXL-97[24] program by minimizing the function $\sum w(F_o^2 - F_c^2)^2$, where F_o and F_c are, respectively, the observed and calculated structure factors. The atomic scattering factors were taken from the international tables for X-ray crystallography.[25] All atoms were located on difference Fourier maps. All non-hydrogen atoms were refined anisotropically except for the sp^2 carbon atoms of **1**. Occupancy factors of an ethanol molecule in **1** were refined to 0.5 and then kept fixed. H atoms were introduced in calculations with the riding model, except those of the water molecules O(10) and O(11) in **2**, which were allowed to vary. Uiso (H) were 1.1 times that of the atom of attachment. H atoms of the disordered O(9) water molecule in **2** were not found. Weighted R-factors, wR, and goodness of fit, S, are based on F_o^2; conventional R-factors, R, are based on F_o, with F_o set to zero for negative F_o^2. Drawings of the molecules were performed with the program ZORTEP[26] with 50% of probability displacement ellipsoids for non-hydrogen atoms. Crystal data collection and refinement parameters are given in Table 1, and selected bond distances and angles are gathered in Tables 2−5.

Physical Measurements. Elemental analyses were carried out at the Laboratoire de Chimie de Coordination Microanalytical Laboratory in Toulouse, France, for C, H, N, and S and at the Service central de Microanalyses du CNRS in Vernaison, France, for Fe. IR spectra were recorded on a GX system 2000 Perkin-Elmer spectrophotometer. Samples were run as KBr pellets.

Mössbauer measurements were obtained on a constant acceleration conventional spectrometer with a 50 mCi source of ^{57}Co (Rh matrix). Isomer shift values (δ) throughout the paper are given with respect to metallic iron at room temperature. The absorber was a sample of 100 mg of microcrystalline powder enclosed in a 20 mm diameter cylindrical plastic sample folder, the size of which had been determined to optimize the absorption. Variable-temperature spectra were obtained in the 4−300 K range by using a MD 306 Oxford cryostat, the thermal scanning being monitored by an Oxford

(21) Boinnard, D.; Cassoux, P.; Petrouleas, V.; Savariault, J.-M.; Tuchagues, J.-P. *Inorg. Chem.* **1990**, *29*, 4114.
(22) Murase, I.; Hatano, M.; Tanaka, M.; Ueno, S.; Okawa, H.; Kida, S. *Bull. Chem. Soc. Jpn.* **1982**, *55*, 2404.
(23) Sheldrick, G. M. *SHELXS-97. Program for Crystal Structure Solution;* University of Göttingen: Göttingen, Germany, 1990.
(24) Sheldrick, G. M. *SHELXL-97: Program for the Refinement of Crystal Structure*; University of Göttingen: Göttingen, Germany, 1997.
(25) *International Tables for Crystallography*; Kluwer Academic Publishers: Dordrecht, The Netherlands, 1992; Vol. C, Tables 4.2.6.8 and 6.1.1.4.
(26) Zolnaï, L. *ZORTEP, Graphical Program for X-ray Structures Analysis*; University of Heilderberg; Germany, 1998.

Table 1. Crystallographic Data for $[Fe_4(pypentO)(pym)_3(Oac)(NCS)_3]\cdot 1.5EtOH$ (**1**), $[Fe_4(pypentO)(pym)(Oac)_2(NCS)_2(MeO)_2(H_2O)]\cdot H_2O$ (**2**), $[Fe_2(pypentO)(NCO)_3]_2$ (**3**), and $[Fe_2(pypentO)(N_3)_3]_2$ (**4**)

formula	$C_{43}H_{53}N_{10}O_{7.5}S_3Fe_4$	$C_{31}H_{45}N_7O_{10}S_2Fe_4$	$C_{40}H_{46}N_{14}O_8Fe_4$	$C_{34}H_{46}N_{26}O_2Fe_4$
fw	1149.53	963.26	1074.31	1074.37
space group	$P2_1/n$ (No. 14)	$C2/c$ (No. 15)	$P2_1/c$ (No. 14)	$P2_1/c$ (No. 14)
a, Å	11.6153(17)	19.9165(17)	11.7633(18)	23.534(3)
b, Å	34.391(17)	21.1001(12)	18.234(3)	18.046(2)
c, Å	14.2150(18)	21.2617(19)	10.4792(16)	10.4865(16)
β, deg	110.88(5)	104.441(10)	99.359(18)	97.80(2)
V, Å^3	5305(3)	8652.7(12)	2217.7(6)	4412.4(10)
Z	4	8	2	4
temp, K	293	180	160	160
λ Å	0.71073	0.71073	0.71073	0.71073
ρ (calcd), g/cm^3	1.439	1.479	1.609	1.617
μ mm^{-1}	1.246	1.467	1.351	1.356
R1[a]	0.0380	0.0305	0.0346	0.0290
wR2 (F^2)[b]	0.1256	0.0789	0.0803	0.0690

[a] $R1 = \sum||F_o| - |F_c||/\sum|F_o|$. [b] $wR2 = \{\sum[w(F_o^2 - F_c^2)^2]/\sum[w(F_o^2)^2]\}^{1/2}$.

Table 2. Selected Interatomic Distances (Å) and Angles (deg) and Torsion Angles (deg) for $[Fe_4(pypentO)(pym)_3(Oac)(NCS)_3]\cdot 1.5EtOH$(**1**)

Fe(1)−O(1)	2.102(4)	Fe(2)−O(1)	2.115(4)
Fe(1)−O(5)	2.264(4)	Fe(2)−O(3)	2.137(5)
Fe(1)−O(6)	2.052(4)	Fe(2)−O(4)	2.040(4)
Fe(1)−N(1)	2.207(6)	Fe(2)−O(6)	2.262(4)
Fe(1)−N(2)	2.175(6)	Fe(2)−N(3)	2.194(6)
Fe(1)−N(8)	2.148(6)	Fe(2)−N(4)	2.182(6)
Fe(3)−O(1)	2.191(4)	Fe(4)−O(4)	2.142(4)
Fe(3)−O(2)	2.104(5)	Fe(4)−O(5)	2.114(4)
Fe(3)−O(4)	2.213(4)	Fe(4)−O(6)	2.169(4)
Fe(3)−O(5)	2.094(4)	Fe(4)−N(6)	2.188(5)
Fe(3)−N(5)	2.173(5)	Fe(4)−N(7)	2.190(5)
Fe(3)−N(9)	2.066(6)	Fe(4)−N(10)	2.111(6)
Fe(1)···Fe(2)	3.1855(15)	Fe(2)···Fe(3)	2.9534(12)
Fe(1)···Fe(3)	3.3260(12)	Fe(2)···Fe(4)	3.3148(15)
Fe(1)···Fe(4)	3.2626(15)	Fe(3)···Fe(4)	3.2421(15)
Fe(1)−O(1)−Fe(2)	98.14(16)	Fe(1)−O(1)−Fe(3)	101.55(17)
Fe(1)−O(5)−Fe(3)	99.42(16)	Fe(1)−O(5)−Fe(4)	96.30(15)
Fe(1)−O(6)−Fe(2)	95.08(16)	Fe(1)−O(6)−Fe(4)	101.20(17)
Fe(2)−O(1)−Fe(3)	86.59(14)	Fe(2)−O(4)−Fe(3)	87.86(15)
Fe(2)−O(4)−Fe(4)	104.81(17)	Fe(2)−O(6)−Fe(4)	96.82(16)
Fe(3)−O(4)−Fe(4)	96.20(16)	Fe(3)−O(5)−Fe(4)	100.77(17)
Fe(1)−O(1)−O(6)−Fe(2)	171.6(2)	Fe(1)−O(1)−O(5)−Fe(3)	178.1(2)
Fe(1)−O(5)−O(6)−Fe(4)	163.5(2)	Fe(2)−O(1)−O(4)−Fe(3)	156.8(2)
Fe(2)−O(4)−O(6)−Fe(4)	179.9(2)	Fe(3)−O(4)−O(5)−Fe(4)	169.4(2)

Table 3. Selected Interatomic Distances (Å) and Angles (deg) and Torsion Angles (deg) for $[Fe_4(pypentO)(pym)(Oac)_2(NCS)_2(MeO)_2(H_2O)]\cdot H_2O$ (**2**)

Fe(1)−O(1)	2.1463(18)	Fe(2)−O(1)	2.1088(19)
Fe(1)−O(2)	2.0889(17)	Fe(2)−O(3)	2.1636(18)
Fe(1)−O(4)	2.0943(17)	Fe(2)−O(5)	2.1090(17)
Fe(1)−O(6)	2.1776(17)	Fe(2)−O(6)	2.1146(17)
Fe(1)−N(1)	2.222(2)	Fe(2)−N(3)	2.219(2)
Fe(1)−N(2)	2.182(2)	Fe(2)−N(4)	2.180(2)
Fe(3)−O(1)	2.1573(18)	Fe(4)−O(2)	2.1759(18)
Fe(3)−O(2)	2.1224(19)	Fe(4)−O(3)	2.1360(18)
Fe(3)−O(3)	2.0943(19)	Fe(4)−O(6)	2.1006(17)
Fe(3)−O(8)	2.1452(18)	Fe(4)−O(7)	2.1075(17)
Fe(3)−O(9)	2.121(10)	Fe(4)−N(5)	2.181(2)
Fe(3)−N(7)	2.224(8)	Fe(4)−N(6)	2.080(2)
Fe(3)−O(9′)	2.106(7)	Fe(3)−N(7′)	2.228(15)
Fe(1)···Fe(2)	2.9574(6)	Fe(2)···Fe(3)	3.2474(6)
Fe(1)···Fe(3)	3.2413(5)	Fe(2)···Fe(4)	3.2463(6)
Fe(1)···Fe(4)	3.2629(6)	Fe(3)···Fe(4)	3.0740(6)
Fe(1)−O(1)−Fe(2)	88.05(7)	Fe(1)−O(1)−Fe(3)	97.73(7)
Fe(1)−O(2)−Fe(3)	100.65(7)	Fe(1)−O(2)−Fe(4)	99.80(7)
Fe(1)−O(6)−Fe(2)	87.09(6)	Fe(1)−O(6)−Fe(4)	99.38(6)
Fe(2)−O(1)−Fe(3)	99.14(8)	Fe(2)−O(3)−Fe(3)	99.39(8)
Fe(2)−O(3)−Fe(4)	98.05(7)	Fe(2)−O(6)−Fe(4)	100.73(7)
Fe(3)−O(2)−Fe(4)	91.31(7)	Fe(3)−O(3)−Fe(4)	93.21(7)
Fe(1)−O(1)−O(6)−Fe(2)	155.36(10)	Fe(1)−O(1)−O(2)−Fe(3)	178.24(10)
Fe(1)−O(2)−O(6)−Fe(4)	177.46(8)	Fe(2)−O(1)−O(3)−Fe(3)	179.70(8)
Fe(2)−O(3)−O(6)−Fe(4)	177.98(9)	Fe(3)−O(2)−O(3)−Fe(4)	156.09(10)

Table 4. Selected Interatomic Distances (Å) and Angles (deg) for $[Fe_2(pypentO)(NCO)_3]_2$ (**3**)

Fe(1)−O(1)	2.0642(18)	Fe(2)−O(1)	1.9698(19)
Fe(1)−N(1)	2.197(2)	Fe(2)−N(3)	2.200(2)
Fe(1)−N(2)	2.189(2)	Fe(2)−N(4)	2.149(2)
Fe(1)−N(5)	2.180(2)	Fe(2)−N(6)	2.019(3)
Fe(1)−N(7)	2.212(2)	Fe(2)−N(7)	2.191(2)
Fe(1)−N(5′)	2.255(2)		
Fe(1)···Fe(2)	3.1764(5)	Fe(1)···Fe(1′)	3.4599(8)
Fe(1)−O(1)−Fe(2)	103.86(8)	Fe(1)−N(7)−Fe(2)	92.35(9)
Fe(1)−N(5)−Fe(1′)	102.54(10)		

ITC4 servocontrol device (±0.1 K accuracy). A least-squares computer program[27] was used to fit the Mössbauer parameters and determine their standard deviations of statistical origin (given in parentheses).

Low magnetic field Mössbauer spectra (up to 0.5 T) were recorded at 4.2 K using a Stöhr cryostat equipped with an electromagnet. The high-field spectra were recorded at 4.2 K using an Oxford cryostat equipped with a superconducting magnet. Both spectrometers operate in the constant acceleration mode using ^{57}Co-(Rh) sources and an external magnetic field perpendicular to the γ-rays. Mössbauer spectral simulations were generated using the WMOSS software package (WEB Research, Edina, MN).

Magnetic data were obtained with a Quantum Design MPMS SQUID susceptometer. All samples were 3 mm diameter pellets molded in the glovebox from ground crystalline samples. Magnetic susceptibility measurements were performed in the 2−300 K temperature range at different magnetic fields between 0.1 and 5 T, and diamagnetic corrections were applied by using Pascal's constants. Isothermal magnetization measurements as a function of the external magnetic field were performed up to 5 T at 2 and 5 K. The magnetic susceptibility has been computed by exact calculation of the energy levels associated with the spin Hamiltonian through diagonalization of the full matrix with a general program for axial symmetry[28] and with the MAGPACK program package[29]

(27) Varret, F. Computer Processing of Mössbauer Spectra. Proceedings of the International Conference on Mössbauer Effect Applications, Jaipur, India, 1981; Indian National Science Academy: New Delhi, 1982.

(28) (a) Aussoleil, J.; Cassoux, P.; de Loth, P.; Tuchagues, J.-P. *Inorg. Chem.* **1989**, *28*, 3051. (b) Theil, S.; Yerande, R.; Chikate, R.; Dahan, F.; Bousseksou, A.; Padhye, S.; Tuchagues, J.-P. *Inorg. Chem*. **1997**, *36*, 6279.

Table 5. Selected Interatomic Distances (Å) and Angles (deg) for $[Fe_2(pypentO)(N_3)_3]_2$ (**4**)

Fe(1)−O(1)	2.0575(16)	Fe(3)−O(2)	2.0427(16)
Fe(1)−N(1)	2.175(2)	Fe(3)−N(5)	2.183(2)
Fe(1)−N(2)	2.192(2)	Fe(3)−N(6)	2.198(2)
Fe(1)−N(9)	2.148(2)	Fe(3)−N(15)	2.208(2)
Fe(1)−N(15)	2.247(2)	Fe(3)−N(18)	2.236(2)
Fe(1)−N(18)	2.169(2)	Fe(3)−N(21)	2.202(2)
Fe(2)−O(1)	1.9659(16)	Fe(4)−O(2)	1.9698(17)
Fe(2)−N(3)	2.184(2)	Fe(4)−N(7)	2.213(2)
Fe(2)−N(4)	2.149(2)	Fe(4)−N(8)	2.156(2)
Fe(2)−N(9)	2.146(2)	Fe(4)−N(21)	2.219(2)
Fe(2)−N(12)	2.087(2)	Fe(4)−N(24)	2.041(2)
Fe(1)···Fe(2)	3.1930(4)	Fe(3)···Fe(4)	3.1447(4)
Fe(1)···Fe(3)	3.4978(5)		
Fe(1)−O(1)−Fe(2)	105.02(7)	Fe(1)−N(9)−Fe(2)	96.07(8)
Fe(1)−N(15)−Fe(3)	103.48(9)	Fe(1)−N(18)−Fe(3)	105.11(9)
Fe(3)−O(2)−Fe(4)	103.19(7)	Fe(3)−N(21)−Fe(4)	90.69(8)

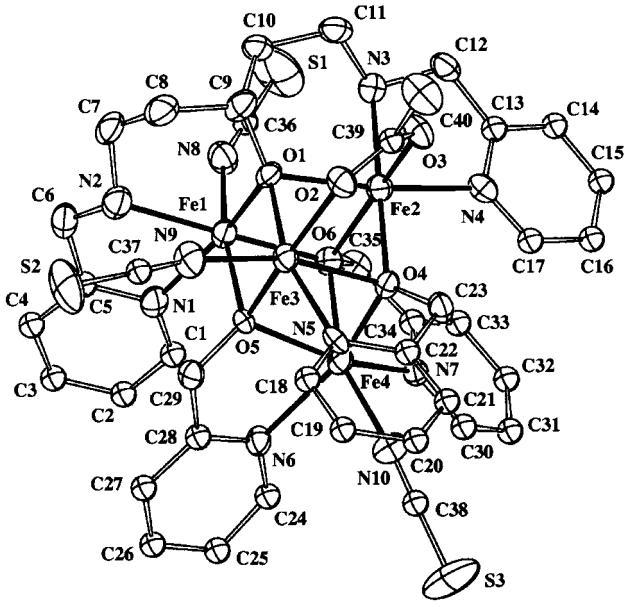

Figure 1. ORTEP view of $[Fe_4(pypentO)(pym)_3(Oac)(NCS)_3]\cdot 1.5EtOH$ (**1**) with atom numbering scheme showing 50% probability ellipsoids.

in the case of rhombic symmetry and magnetization curves. The powder susceptibilities have been determined by using the classical expression taking into account the contributions of the principal axes ($1/3z + 2/3xy$) and through integration over all orientations of the external magnetic field with respect to the sample. Least-squares fittings were accomplished with an adapted version of the function-minimization program MINUIT.[30]

Results and Discussion

Description of the Structures. The molecular structure of complex **1** is shown in Figure 1. The unit cell includes four tetranuclear complex molecules and six ethanol molecules as crystallization solvent, and the crystal packing results from hydrogen contacts between adjacent complex molecules.[31] Each complex molecule consists of a cubane-like arrangement of four iron atoms, four μ_3-O-alkoxo bridging ligands (one pypentO and three pym), one syn−syn bridging acetate, and three terminal monodentate NCS^- ligands. The coordination sphere of the four Fe^{II} centers is distorted octahedral, but each iron possesses a different ligand environment: N_3O_3 donor set to Fe1 with N_{py}(pypentO), N_{amine}(pypentO), N(NCS^-), μ_3-O_{alkoxo}(pypentO), and two μ_3-O_{alkoxo}(pym); N_3O_3 donor set to Fe4 with two N_{py}(pym), N(NCS^-), and three μ_3-O_{alkoxo}(pym); N_2O_4 donor set to Fe2 with N_{py}(pypentO), N_{amine}(pypentO), μ-Oac, μ_3-O_{alkoxo}(pypentO), and two μ_3-O_{alkoxo}(pym); and N_2O_4 donor set to Fe3 with N_{py}(pym), N(NCS^-), μ-Oac, μ_3-O_{alkoxo}(pypentO), and two μ_3-O_{alkoxo}(pym). The variety of ligands involved results in a cubane structure devoid of any point group element of symmetry. However, with only the Fe_4O_4 core and the nature of the bridging ligands for the different faces of the cube taken into account, it is possible to roughly assume a D_{2d} point group symmetry. In this elongated cube, four Fe···Fe long distances (3.19−3.33 Å) correspond to the faces including two μ_3-OR bridges, and the Fe2···Fe3 short distance (2.95 Å) corresponds to the face including two μ_3-OR bridges and one acetate bridge. The face opposite to this one has a long Fe1···Fe4 distance (3.26 Å) but differs from the set of four faces previously mentioned by an Fe−O−O−Fe dihedral angle far below 180°.

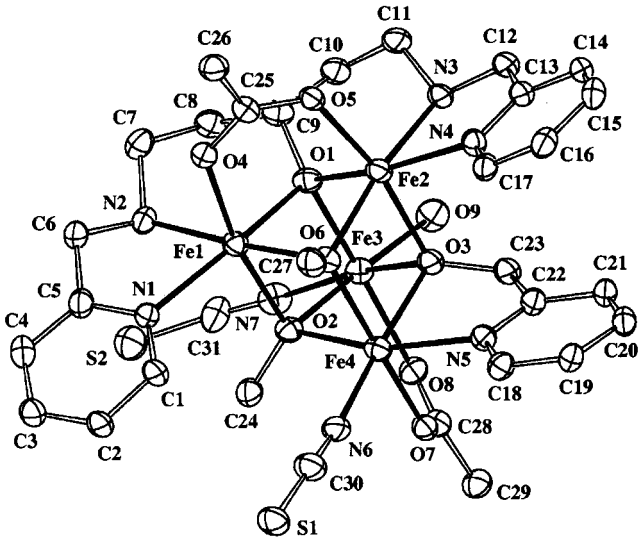

Figure 2. ORTEP view of $[Fe_4(pypentO)(pym)(Oac)_2(NCS)_2(MeO)_2(H_2O)]\cdot H_2O$ (**2**) with atom numbering scheme showing 50% probability ellipsoids.

The molecular structure of complex **2** is shown in Figure 2. The unit cell includes eight tetranuclear complex molecules and eight water molecules as crystallization solvent, and the crystal packing results from hydrogen contacts between adjacent complex molecules.[31] Each complex molecule consists of a cubane-like arrangement of four iron atoms, four μ_3-O-alkoxo bridging ligands (one pypentO, one pym, and two OMe), two syn−syn bridging acetates, and three terminal monodentate ligands (two NCS^- and one H_2O). The coordination sphere of the four iron is distorted octahedral, but each Fe^{II} possesses a different ligand environment: N_2O_4 donor set to Fe1 with N_{py}(pypentO), N_{amine}(pypentO), μ-Oac, μ_3-O_{alkoxo}(pypentO), and two μ_3-OMe; N_2O_4 donor set to Fe2

(29) (a) Borrás-Almenar, J. J.; Clemente-Juan, J. M.; Coronado, E.; Tsukerblat, B. S. *Inorg. Chem.* **1999**, *38*, 6081. (b) Borrás-Almenar, J. J.; Clemente-Juan, J. M.; Coronado, E.; Tsukerblat, B. S. *J. Comput. Chem.* **2001**, *22*, 985−991.

(30) James, F.; Roos, M. *MINUIT Program, a System for Function Minimization and Analysis of the Parameters Errors and Correlations*; *Comput. Phys. Commun.* **1975**, *10*, 345.

(31) See Supporting Information.

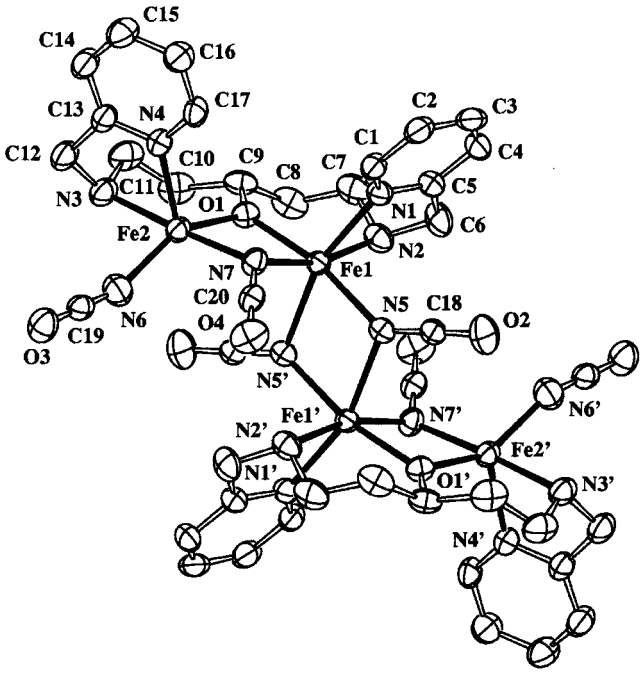

Figure 3. ORTEP view of $[Fe_2(pypentO)(NCO)_3]_2$ (**3**) with atom numbering scheme showing 50% probability ellipsoids.

with N_{py}(pypentO), N_{amine}(pypentO), μ-Oac, μ_3-O_{alkoxo}(pypentO), μ_3-O_{alkoxo}(pym), and μ_3-OMe; N_2O_4 donor set to Fe4 with N_{py}(pym), N(NCS^-), μ-Oac, μ_3-O_{alkoxo}(pym), and two μ_3-OMe; and NO_5 donor set to Fe3 with N(NCS^-), O_W, μ-Oac, μ_3-O_{alkoxo}(pypentO), μ_3-O_{alkoxo}(pym), and μ_3-OMe. The thiocyanate anion and the water molecule are disordered among their two Fe3 coordination sites with occupancy factors equal to 0.5. Despite the presence of two acetate bridges, the number of different ligands involved results in a cubane structure devoid of any point group element of symmetry, similarly to **1**. With only the Fe_4O_4 core and the nature of the bridging ligands for the different faces of the cube taken into account, it is possible to assume a D_{2d} symmetry. In this elongated cube, the four Fe···Fe long distances (3.24−3.26 Å) correspond to the faces of the cube including two μ_3-OR bridges, and the two Fe···Fe short distances (2.96 and 3.07 Å) correspond to the faces including two μ_3-OR bridges and one acetate bridge.

The molecular structure of complex **3** is shown in Figure 3. The unit cell includes two tetranuclear complex molecules, and the crystal packing results from hydrogen contacts between adjacent complex molecules.[31] Each complex molecule consists of a zigzag arrangement of four iron(II) cations, two μ_2-O bridging pypentO ligands, four μ_2-N-cyanato bridging ligands, and two terminal monodentate NCO^- anions. This new type of tetranuclear iron(II) structure results from the bridging of two Fe_2(pypentO)$(NCO)_2$ dinuclear moieties through two μ_2-N-cyanato anions. Each constituting Fe_2(pypentO)$(NCO)_2$ unit results from the bridging of two iron(II) atoms through one μ_2-N-cyanato anion and the central O_{alkoxo} of the pentadentate pypentO^- ligand. The two Fe_2(pypentO)$(NCO)_2$ units are related by symmetry through an inversion center situated at the barycenter of the complex. The distorted octahedral coordination sphere of the

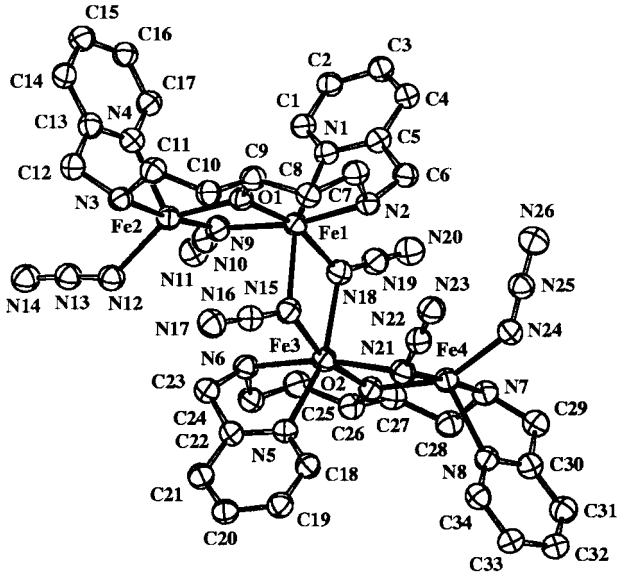

Figure 4. ORTEP view of $[Fe_2(pypentO)(N_3)_3]_2$ (**4**) with atom numbering scheme showing 50% probability ellipsoids.

internal iron (Fe1) involves a N_5O donor set including: N_{py}(pypentO), N_{amine}(pypentO), three μ_2-N(NCO^-), and μ_2-O_{alkoxo}(pypentO). The pentagonal coordination sphere of the external iron (Fe2) is intermediate between a trigonal bipyramid and a square pyramid with a N_4O donor set including N_{py}(pypentO), N_{amine}(pypentO), N(NCO^-), μ_2-N(NCO^-), and μ_2-O_{alkoxo}(pypentO). The distortion of the coordination polyhedron around Fe2 can be quantified using the approach of Muetterties and Guggenberger.[32] In this method, the dihedral angles between adjacent faces (known as shape-determining angles e_1, e_2, and e_3) are calculated in order to describe an intermediate geometry. The key shape-determining angle, e_3, is equal to 0° for an ideal square pyramid and 53.1° for an ideal trigonal bipyramid. e_3 is equal to 30.53° for the Fe2 site, confirming that the departure from the ideal trigonal bipyramid is significant. The intradinuclear Fe1···Fe2 and interdinuclear Fe1···Fe1′ distances between adjacent iron centers are 3.18 and 3.46 Å, respectively.

The molecular structure of complex **4** is shown in Figure 4. The unit cell includes four tetranuclear complex molecules, and the crystal packing results from hydrogen contacts between adjacent complex molecules.[31] Similarly to **3**, each complex molecule consists of a zigzag arrangement of four iron(II) cations, two μ_2-O bridging pypentO ligands, four μ-1,1-N-azido bridging ligands, and two terminal monodentate N_3^- anions. Similarly to complex **3**, this tetranuclear iron(II) structure results from the bridging of two Fe_2(pypentO)$(N_3)_2$ dinuclear moieties through two μ-1,1-azido anions. However, the symmetry is lower in complex **4** due to the loss of the inversion center: the four iron(II) sites are crystallographically independent. This lower symmetry results from a significant difference in the coordination sphere of the external iron atoms. While the Fe1 and Fe3 internal iron sites are almost equivalent, the Fe2 and Fe4 external ones differ in the pseudo-coordination with one of the N_3

(32) Muetterties, E. L.; Guggenberger, L. J. *J. Am. Chem. Soc.* **1974**, *96*, 1748.

bridging anions connecting the two internal irons: the Fe2···N17 distance is 3.085(3) Å, while the Fe4···N20 distance is 3.479(3) Å. Each constituting $Fe_2(pypentO)(N_3)_2$ unit results from the bridging of two iron(II) atoms through one μ-1,1-N-azido anion and the central O_{alkoxo} of the pentadentate pypentO$^-$ ligand. The distorted octahedral coordination sphere of the internal irons (Fe1, Fe3) involves a N_5O donor set including N_{py}(pypentO), N_{amine}(pypentO), three μ-1,1-N(N_3^-), and μ_2-O_{alkoxo}(pypentO). The pentagonal coordination sphere of the external irons (Fe2, Fe4) is intermediate between a trigonal bipyramid and a square pyramid with a N_4O donor set including N_{py}(pypentO), N_{amine}(pypentO), N(N_3^-), μ-1,1-N(N_3^-), and μ_2-O_{alkoxo}(pypentO). The key shape-determining angle,[32] e_3, is equal to 31.45 and 26.23° for the Fe2 and Fe4 site, respectively, confirming that the departure from the ideal trigonal bipyramid is significant for both sites, but larger for the Fe4 site. The stronger Fe2···N17 pseudo-coordination (3.085 Å) is better accommodated with a smaller tetragonal distortion (e_3, = 31.45°), while the weaker Fe4···N20 pseudo-coordination (3.479 Å) is better-accommodated with a larger tetragonal distortion (e_3, = 26.23°). The Fe1···Fe2 and Fe3···Fe4 intradinuclear distances and the Fe1···Fe3 interdinuclear distance between adjacent iron centers are 3.19, 3.14, and 3.50 Å, respectively.

The four structures described above clearly evidence that the same synthetic procedure leads to very different structural types as a result of the effect of the pseudo-halide anion. While in the presence of NCS anions, low-symmetry Fe_4O_4 cubane-like structures including only one bridging pentadentate ligand (pypentO) are obtained (**1**, **2**); Fe_4 complex molecules consisting of two N-bridged dinuclear units, each including one bridging pentadentate ligand (pypentO), are obtained when NCO or N_3 anions are present (**3**, **4**). The cubane-like arrangement of four iron(II) and four μ_3-O atoms has previously been described.[13,16] However, at variance with the case of complexes **1** and **2**, the four Fe^{II} have the same ligand environment and are thus equivalent in the previously reported cubane-like Fe^{II} compounds. Complexes **1** and **2** include the first low-symmetry Fe_4O_4 cubane cores in which the four iron(II) centers are nonequivalent. A low-symmetry Ni_4O_4 cubane-like structure very similar to that of complex **2** has been recently reported that also involves the bridging pentadentate ligand (pypentO).[33] Tetranuclear ferrous complexes consisting of two N-bridged dinuclear units are unprecedented, and a zigzag array of four irons has only been described with *O*-catecholate bridges.[20] Complexes **3** and **4** are thus the first examples of a new class of tetranuclear iron compounds.

Mössbauer Spectroscopy. Mössbauer spectra of polycrystalline samples of **1**−**4** are presented in Figures 5 and 8−10, and the parameters resulting from the fit of selected spectra are collected in Table 6.

The spectra of complex **1** show a composite high-spin iron(II) quadrupole-split doublet with different shoulder features as a function of temperature. Crystallographically, complex

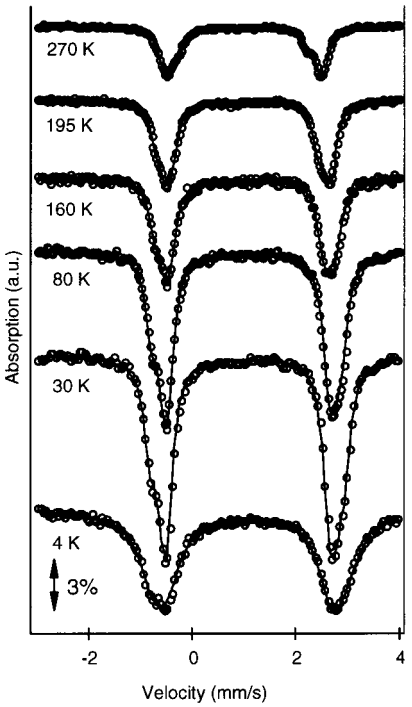

Figure 5. Representative Mössbauer spectra of $[Fe_4(pypentO)(pym)_3(Oac)(NCS)_3]\cdot 1.5EtOH$ (**1**).

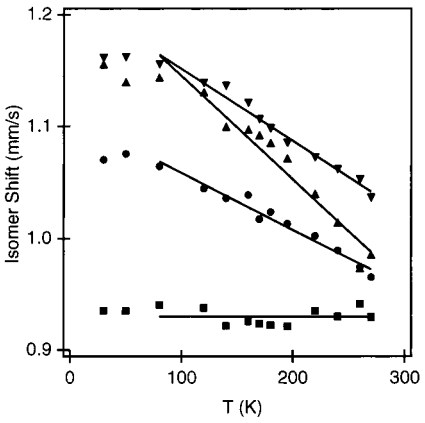

Figure 6. Temperature dependence of the isomer shift for the four iron(II) sites of $[Fe_4(pypentO)(pym)_3(Oac)(NCS)_3]\cdot 1.5EtOH$ (**1**).

1 has four iron(II) sites differing not only in the N/O ratio of their coordination sphere (two N_3O_3 and two N_2O_4) but also in the chemical nature of the N and O donors for a given type of donor set (N_3O_3 or N_2O_4). The four quadrupole-split doublets are partially superimposed in the spectra and can only be distinguished and identified through a detailed study of their temperature dependence. The spectra obtained at 15 temperatures between 4 and 270 K have been satisfactorily fitted with four single quadrupole-split doublets of an equal area ratio that can be attributed to the different iron sites of the Fe_4O_4 cube. It is remarkable that attempts to fit these Mössbauer spectra with two or three quadrupole-split doublets failed. The parameters resulting from the best fits over the full temperature range are plotted in Figures 6 and 7. The isomer shift, δ, and quadrupole splitting parameters, ΔE_Q, are consistent with four high-spin iron(II) sites. Two different sets of isomer shift values, $\delta \sim 1.08$ mm/s (sites **1a** and **1b** with N_3O_3 donor sets) and $\delta \sim 1.15$ mm/s (sites

(33) Clemente-Juan, J. M.; Chansou, B.; Donnadieu, B.; Tuchagues, J.-P. *Inorg. Chem.* **2000**, *39*, 5515−5519.

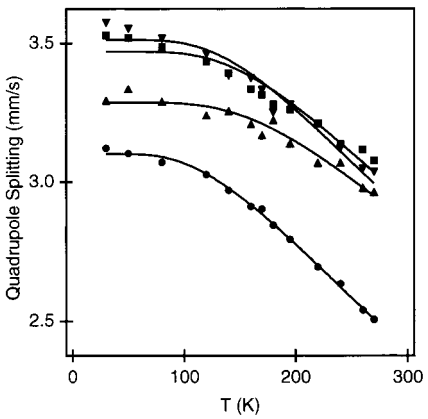

Figure 7. Temperature dependence of the quadrupole splitting for the four iron(II) sites of $[Fe_4(pypentO)(pym)_3(Oac)(NCS)_3]\cdot 1.5EtOH$ (**1**). The solid lines correspond to the fits taking into account the contribution of each low-lying T_{2g} level to the quadrupole splitting.[35,36]

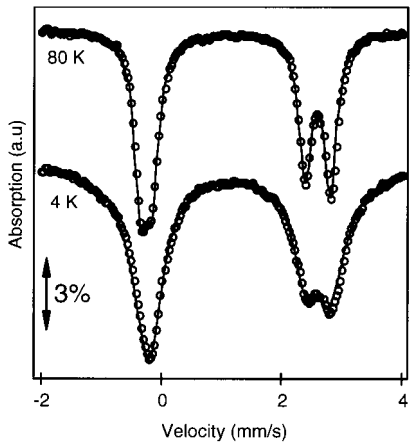

Figure 8. Representative Mössbauer spectra of $[Fe_2(pypentO)(NCO)_3]_2$ (**3**).

1c and **1d** with N_2O_4 donor sets), are observed at 270 K. The temperature dependence of δ (Figure 6) is approximately linear, corresponding to second-order Doppler effect behavior. However, it is very different for the four sites, illustrating not only the difference in the N/O ratio of their coordination sphere (two N_3O_3 and two N_2O_4) but also the difference in the chemical nature of the N and O donors for a given type of donor set (**1a** and **1b** for N_3O_3 or **1c** and **1d** for N_2O_4).[34] The values of the quadrupole splittings, ΔE_Q, are in the 3−4 mm/s range at low temperatures, indicating that the strongly distorted octahedral iron(II) sites have a singlet ground state. Figure 7 shows the temperature dependence of the quadrupole splittings for the four sites. ΔE_Q values decrease rapidly with increasing temperature due to the population of the low-lying energy levels, close in energy due to the low symmetry of the sites and spin−orbit interactions. This behavior can be fitted by taking into account the Boltzmann population of the low-lying levels (T_{2g}) and the individual contribution of each level to the quadrupole splitting.[35] The ratio between the average energy splittings between the fundamental and the first excited orbital states for two sites of similar ligand environments (ΔE_{1a} and ΔE_{1b} for N_3O_3, and ΔE_{1c} and ΔE_{1d} for N_2O_4) gives a rough estimate of the relative degree of their distortion and can be evaluated from the thermal variation of their quadrupole splittings.[36] Fitting the thermal variation of the quadrupole splittings yields the ratios $\Delta E_{1a}/\Delta E_{1b} = 0.822$ and $\Delta E_{1d}/\Delta E_{1c} = 0.900$ ($\Delta E = 500$, 609, 635, and 571 cm^{-1} and $\Delta E_Q(0\ K) = 3.03$, 3.41, 3.25, and 3.44 mm/s for sites 1a, 1b, 1c, and 1d, respectively ($\Delta E_Q = \Delta E_Q(0\ K)\tanh(\Delta E/2kT)$)). The differences in $\Delta E_Q(0\ K)$ values for the different sites result from the thermally independent term of the quadrupole splitting, which depends on the network contributions and not on the thermal population of electronic levels.

Table 6. Representative Least-Squares-Fitted Mössbauer Data for $[Fe_4(pypentO)(pym)_3(Oac)(NCS)_3]\cdot 1\cdot 5EtOH$ (**1**), $[Fe_4(pypentO)(pym)(Oac)_2(NCS)_2(MeO)_2(H_2O)]\cdot H_2O$ (**2**), $[Fe_2(pypentO)(NCO)_3]_2$ (**3**), and $[Fe_2(pypentO)(N_3)_3]_2$ (**4**)

compnd site (donor set)	T (K)	area ratio (%)	δ ($mm\cdot s^{-1}$)	$\Gamma/2$ ($mm\cdot s^{-1}$)	ΔE_Q ($mm\cdot s^{-1}$)
1a (N_3O_3)	270	25[a]	1.092(2)	0.13(2)[b]	2.505(5)
1a (N_3O_3)	180	25[a]	1.152(4)	0.13(2)[b]	2.84(1)
1a (N_3O_3)	80	25[a]	1.192(5)	0.13(2)[b]	3.07(1)
1b (N_3O_3)	270	25[a]	1.06(1)	0.13(2)[b]	3.08(1)
1b (N_3O_3)	180	25[a]	1.050(4)	0.13(2)[b]	3.280(8)
1b (N_3O_3)	80	25[a]	1.068(2)	0.13(2)[b]	3.486(5)
1c (N_2O_4)	270	25[a]	1.12(1)	0.13(2)[b]	2.96(2)
1c (N_2O_4)	180	25[a]	1.21(1)	0.13(2)[b]	3.22(2)
1c (N_2O_4)	80	25[a]	1.272(6)	0.13(2)[b]	3.29(1)
1c (N_2O_4)	270	25[a]	1.17(1)	0.13(2)[b]	3.04(1)
1d (N_2O_4)	180	25[a]	1.23(1)	0.13(2)[b]	3.25(2)
1d (N_2O_4)	80	25[a]	1.284(2)	0.13(2)[b]	3.526(5)
2	80	100	1.192(2)	0.190(4)	3.047(5)
2	293	100	1.099(8)	0.19(1)	2.46(2)
3a (N_5O)	80	52.6(3)	1.085(1)	0.126(1)	2.461(1)
3b (N_4O)	80	47.4(3)	1.196(1)	0.126(1)	3.047(1)
4a (N_5O)	270	39.1(6)	0.980(2)	0.128(2)	2.487(5)
4a (N_5O)	180	44(8)	1.052(2)	0.135(4)	2.47(2)
4a (N_5O)	150	48(2)	1.050(5)	0.132(4)	2.518(8)
4a (N_5O)	80	51.7(5)	1.046(1)	0.134(1)	2.530(2)
4b (N_4O)	270	60.9(6)	1.046(1)	0.128(2)	1.927(3)
4b (N_4O)	180	28.4(8)	1.107(4)	0.135(4)	2.026(9)
4b (N_4O)	150	25.9(8)	1.122(4)	0.132(4)	2.086(9)
4b (N_4O)	80	23.4(4)	1.251(3)	0.134(1)	2.443(5)
4c (N_4O)	180	27(8)	1.059(4)	0.135(4)	2.65(3)
4c (N_4O)	150	26(2)	1.100(5)	0.132(4)	2.79(1)
4c (N_4O)	80	24.9(3)	1.144(2)	0.134(1)	3.174(4)

[a] Area ratios have been set to 25%. [b] A common value of $\Gamma/2$ (allowed to vary) has been imposed to sites **1a**−**d**.

The spectra of complex **2** also show a composite high-spin iron(II) quadrupole-split doublet (not shown). However, at variance with the case of complex **1**, the constituting quadrupole-split doublets cannot be distinguished. The parameters resulting from the best fits at 293 and 80 K are collected in Table 6. The isomer shift, δ, and quadrupole splitting parameters, ΔE_Q, are close to those obtained for complex **1** and consistent with high-spin iron(II) sites. ΔE_Q values (3.05 mm/s at 80 K) indicate that the strongly distorted octahedral iron(II) sites have a singlet ground state. As in the case of complex **1**, ΔE_Q decreases with increasing temperature, reaching 2.46 mm/s at 293 K due to the population of the low-lying energy-levels, close in energy.

(34) Greenwood, N. N.; Gibbs, T. C. *Mössbauer Spectroscopy*; Chapman and Hall: New York, 1971.
(35) Ingalls, R. *Phys. Rev.* **1964**, *133A*, 787.
(36) (a) Ducouret-Cérèse, A.; Varret, F. *J. Phys.* (Paris) **1988**, *49*, 661−666. (b) Boinnard, D.; Bousseksou, A.; Dworkin, A.; Savariault, J. M.; Varret, F.; Tuchagues, J. P. *Inorg. Chem.* **1994**, *33*, 271−281.

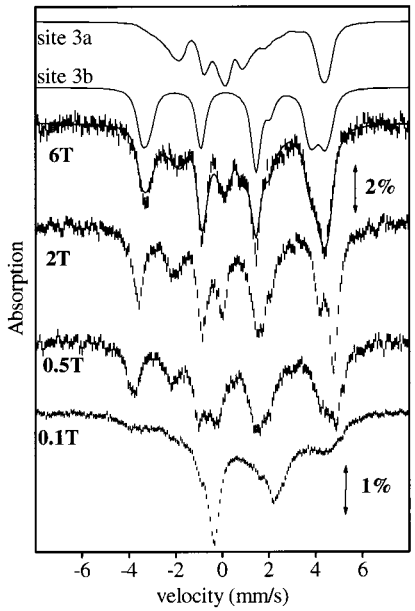

Figure 9. Mössbauer spectra of complex **3** in the presence of external magnetic fields at 4.2 K. Solid lines above the 6 T spectrum are sub-site simulations generated from an $S = 2$ spin Hamiltonian. The following parameters were used to generate the simulations: $D = -7.6$ cm^{-1}, $E/D = 0.33$, $\tilde{A} = (-34, -34, -13)$ MHz, $\Delta E_Q = +2.50$ mm/s, $\delta = 1.08$ mm/s, $\eta = 0.44$, $\alpha = 86°$, $\beta = 21°$ (site **3a**), and $D = -7.6$ cm^{-1}, $E/D = 0.33$, $\tilde{A} = (-34, -34, -17)$ MHz, $\Delta E_Q = +2.94$ mm/s, $\delta = 0.28$ mm/s, $\eta = 0$, $\alpha = 90°$, $\beta = 80°$ (site **3b**), where α and β are polar angles describing the orientations of the EFG-tensors relative to the tensor of the zero-field splitting. We emphasize that the quoted parameters indicate the existence of two distinct ferrous ions.

For the purpose of comparison, we have fitted the 80 K Mössbauer spectrum of complex **1** with only one quadrupole split doublet: indeed, the parameters obtained, $\delta = 1.214(2)$, $\Delta E_Q = 3.310(5)$, and $\Gamma/2 = 0.22(4)$ mm/s, are similar to those obtained for complex **2** at 80 K (Table 6).

The spectra of complex **3** include two partially superimposed quadrupole-split doublets of an equal area ratio (Figure 8). The δ and ΔE_Q parameters are consistent with two quite different high-spin iron(II) sites (**3a**, N_5O; **3b**, N_4O) in the complex (Table 6). At 4 K, in the absence of an applied magnetic field, the two doublets are broadened. Figure 9 shows Mössbauer spectra for complex **3** recorded at 4.2 K in the presence of external magnetic fields. Sizable magnetic hyperfine interactions are already induced by a weak applied field of 0.1 T. This observation implies that the electronic spin relaxation rates at 4.2 K are relatively slow compared to the nuclear precession frequencies. The internal magnetic field appears to saturate for relatively weak fields. The high-field spectra consist of reasonably sharp lines. On the basis of theoretical considerations developed elsewhere,[37,38] the behavior of the spectra is characteristic of an electronic system with integer spin for which the splitting between the two lowest sublevels, Δ_{ground}, is small (for a multiplet with spin S, the $M = \pm S$ doublet splits through mixing by the $E(S_x^2 - S_y^2)$term). The broadening observed for the zero field

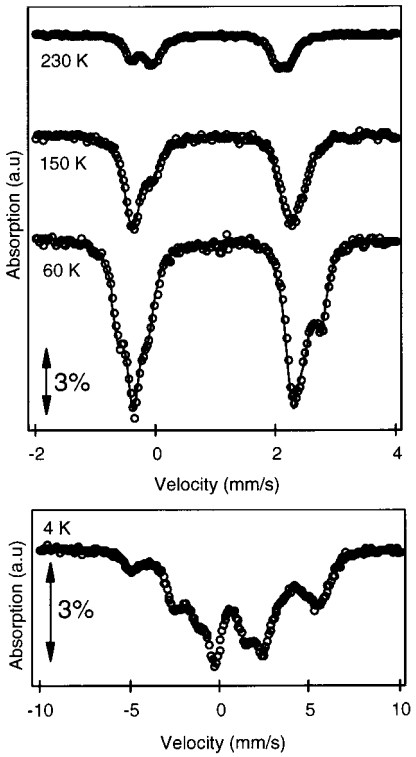

Figure 10. Representative Mössbauer spectra of $[Fe_2(pypentO)(N_3)_3]_2$ (**4**).

spectra at 4.2 K suggests that Δ_{ground} is substantially small ($\sim$0.1 cm^{-1}). For small Δ_{ground} values, line broadening results from mixing of the two electronic levels induced by magnetic hyperfine interactions.[38] A unique set of parameters that fits the spectra cannot be identified due to the large number of unknowns. The solid lines above the 6 T spectrum in Figure 9 are simulations generated assuming an $S = 2$ spin Hamiltonian. This approach, although not strictly correct if the complete interaction is to be taken into account, gives us hints concerning the magnetic properties of the ferrous ions. The simulations show that the two ferrous ions have substantially different magnetic hyperfine splittings. The species with the larger ΔE_Q, namely, site **3b**, exhibits the largest magnetic splitting.

The low-temperature spectra (20−180 K) of complex **4** show a composite quadrupole-split doublet (Figure 10). This composite signal can be fitted with three quadrupole-split doublets with 1:2:1 area ratios. The δ and ΔE_Q parameters are consistent with the presence of three high-spin iron(II) sites (**4a**, N_5O; **4b** and **4c**, N_4O) in this complex (Table 6). Above 180 K, the spectra resemble a pair of quadrupole-split doublets and the convolution model for three quadrupole-split doublets with 1:2:1 intensities does not reproduce the experimental spectra. Observation of three different iron(II) sites below 180 K is consistent with the difference in symmetry of the coordination sphere of the external iron sites Fe2 and Fe4 evidenced by the structural study at 160 K. At temperatures higher than 180 K, the tiny difference in the coordination sphere of Fe2 and Fe4 may no longer be observable due to thermal motion. At 4 K, the spectrum (Figure 10) presents a magnetic hyperfine structure in the absence of an applied field, indicating either the presence

(37) Münck, E.; Surerus, K. K.; Hendrich, M. P. *Methods Enzymol.* **1993**, *277*, 463.
(38) Surerus, K. K.; Hendrich, M. P.; Christie, P. D.; Rottgardt, D.; Orme-Johnson, W. H.; Münck, E. *J. Am. Chem. Soc.* **1992**, *114*, 8579.

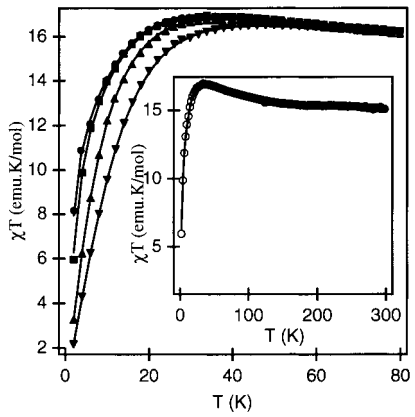

Figure 11. $\chi_M T$ product vs T under applied magnetic fields of 0.5, 0.9, 2.5, and 5 T for $[Fe_4(pypentO)(pym)_3(Oac)(NCS)_3]\cdot 1.5EtOH$ (**1**). Solid lines represent the best simultaneous fit of the four sets of data with the D_{2d} symmetry model including single-ion ZFS (see text).

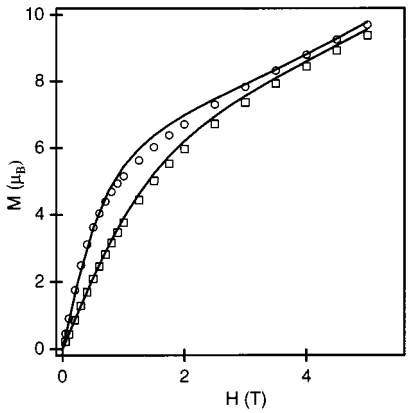

Figure 12. M vs H curves at 2 and 5 K for complex **1**. Solid lines represent the calculated curves from the best fits of $\chi_M T$ vs T shown in Figure 11.

of magnetic ordering or a slow relaxation regime with $\Delta_{ground} \sim 0$ (smaller than that estimated for **3**) yielding a full magnetic spectrum.[38]

Magnetic Properties. The thermal variation of the magnetic susceptibility (χ) at different magnetic fields and the isothermal magnetization at low temperatures have been measured for complexes **1**−**4**. The electronic ground state of iron(II) in these compounds is orbitally degenerate ($^4T_1$). The magnetism of exchange-coupled transition-metal ions with this type of ground state is very complicated, and it is an open problem for which no general solution is available.[39] To study the present systems we have assumed that a simple Hamiltonian with isotropic exchange interactions between the spins and single-ion anisotropy associated to the spin of each center is valid. This model implies that the orbital contributions are taken into account within the effective zero-field splitting parameter, D.

The temperature dependence of χT at different fields for complex **1** is plotted in Figure 11. The χT product measured under a magnetic field of 0.9 T increases with decreasing temperature from 15 emu K mol^{-1} at 300 K up to a round maximum at 17 K. The position and height of this maximum depends on the applied magnetic field. When the magnetic field is increased, the maximum shifts to higher temperatures and its height decreases. This results from an additional splitting of the energy levels due to the Zeeman effect. The magnetization curves at low temperatures (2 and 5 K) (Figure 12) do not show a clear saturation value in agreement with a poorly isolated spin ground state: an intricate scheme of energy levels is then expected. The temperature dependence of χT for **1** was fitted using the following Hamiltonian:

$$\hat{H} = -2J_1(\hat{S}_1\hat{S}_2 + \hat{S}_1\hat{S}_3 + \hat{S}_2\hat{S}_4 + \hat{S}_3\hat{S}_4) - 2J_2\hat{S}_2\hat{S}_3 - 2J_3\hat{S}_1\hat{S}_4 + D(\hat{S}_{z1}^2 + \hat{S}_{z2}^2 + \hat{S}_{z3}^2 + \hat{S}_{z4}^2) \quad (1)$$

Analytical expressions for eigenvalues and susceptibility cannot be derived due to the ZFS term. To calculate the energy levels and magnetic properties, diagonalization of the full matrix has been carried out.[28] A low-symmetry model (D_{2d}) is suggested by the differences in structural parameters among the faces of the cube (Figure 13). The corresponding network of exchange pathways is also shown in Figure 13: the exchange interaction J_2 is associated with the face including two μ_3-OR bridges and one acetate bridge, J_3 is associated with the opposite face, and the average exchange parameter J_1 is associated with the four other faces assumed to be equivalent. The best fit for the 0.9 T curve (not shown) was obtained for the following set of parameters: $J_1 = 0.4$ cm^{-1}, $J_2 = -2.7$ cm^{-1}, $J_3 = 4.4$ cm^{-1}, $D = 6.4$ cm^{-1}, $g = 2.21$, and a residual $R = 6.8 \times 10^{-4}$. The same set of parameters simulates the 0.5 T curve with good agreement, but this set of parameters failed to simulate the high-field curves (2.5 and 5.0 T). Similarly, the low-temperature magnetization data cannot be satisfactorily simulated with this set of parameters. Only the low-field range is well reproduced, while the high-field range is overestimated. To refine the parameters obtained and discriminate between the splitting associated with the effect of the magnetic field and single-ion anisotropy, a simultaneous fit of the χT curves at different fields has been performed. The best fit for the

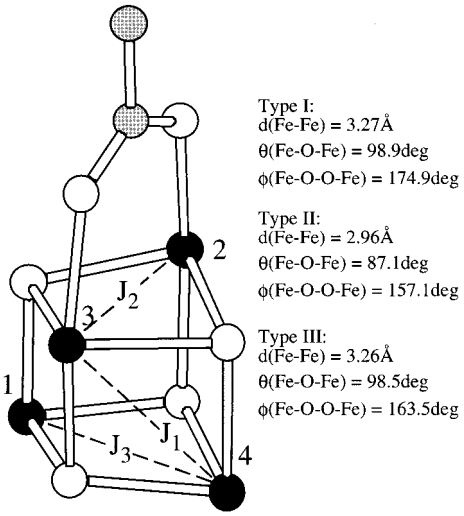

Figure 13. Schematic view of the $Fe_4O_4(Oac)$ core of complex **1**. Filled balls denote iron atoms, and empty ones denote bridging oxygen atoms or acetate groups. Dashed lines show the three types of Fe···Fe exchange interactions (J_1, J_2, and J_3) based on the differences in structural parameters.

(39) Borrás-Almenar, J. J.; Clemente-Juan, J.-M.; Coronado, E.; Palii, A.; Tsukerblat, B. S. *J. Phys. Chem. A* **1998**, *102*, 200.

complete set of curves was obtained for parameters qualitatively similar to those obtained from the fit of the 0.9 T curve. The 2 and 5 K magnetization curves simulated with this set of parameters are qualitatively correct: the curve shape is satisfactorily reproduced; however, the theoretical curves are above the experimental data in the overall magnetic field range. This may originate from the fact that the magnetic susceptibility data have been fitted by taking into account only the principal axes, while the fitting of magnetization curves has been performed through integration over all orientations of the axis of anisotropy with respect to the applied magnetic field. In the case of highly anisotropic systems, evaluating these two magnetic properties differently may introduce significant disagreements. We therefore decided to perform a simultaneous fit of the χT data at different fields through integration over all orientations of the axis of anisotropy with respect to the magnetic field. The best fit for the complete set of curves was obtained for the following set of parameters: $J_1 \sim 0$ cm^{-1}, $J_2 = -1.3$ cm^{-1}, $J_3 = 4.6$ cm^{-1}, $D = 6.4$ cm^{-1}, $g = 2.21$, and a residual $R = 6.8 \times 10^{-3}$ (solid lines in Figure 11). Attempts to fit with rhombic anisotropy yielded an almost identical set of parameters and an E/D ratio smaller than 1×10^{-4}. The 2 and 5 K magnetization data were then satisfactorily simulated with this set of parameters (solid lines in Figure 12): all energy levels obtained with the set of exchange and ZFS parameters obtained from the fit of the complete set of susceptibility curves have been taken into account, and diagonalization of the full matrix has been performed at each value of the magnetic field for calculation of the theoretical curves.[29a] The results from these simultaneous fits confirm that the interactions are ferromagnetic between irons bridged by two μ_3-OR oxygen atoms (J_3) and antiferromagnetic between irons bridged by two μ_3-OR oxygen atoms and one acetate anion. The exchange pathway through two μ_3-OR oxygen atoms yields an exchange integral J_1 close to zero, indicating that the magnetic interactions in this tetranuclear core may be explained with a model including two different dinuclear cores interacting weakly. The resulting scheme of energy levels (Figure SI-1) is quite complex, and there is not a well-isolated spin manifold split by zero-field splitting. This complex structure of energy levels originates from two factors: (i) competition between ferromagnetic and antiferromagnetic interactions, which yields an intermediate spin-state, and (ii) comparable absolute magnitudes for J and D. The change in nature between the J_2 (antiferromagnetic) and J_3 (ferromagnetic) interactions has been observed in previously described iron alkoxide cubes for which the authors[13] evidenced a ferromagnetic exchange interaction (0.94 cm^{-1}) for highly symmetrical (T_d) iron(II) cubes, $\{Fe_4(OMe)_4\}^{4+}$. In the same work a trapped mixed-valence iron(II)−iron(III) cube, $\{Fe_4(OMe)_4\}^{5+}$, was shown to exhibit antiferromagnetic behavior with $J(Fe^{II}-Fe^{II}) = -1.3$ cm^{-1}. Taft et al.[13] obtained this parameter with an isotropic Hamiltonian and a fit of the χT curve performed only above 30 K, implying that the effect of the zero-field splitting contribution observed at low temperature was neglected. Consequently, the absolute value of the parameters obtained by Taft et al.

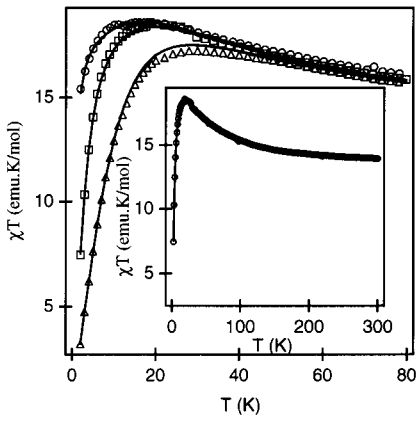

Figure 14. $\chi_M T$ product vs T under applied magnetic fields of 0.5, 0.9, 2.5, and 5 T for $[Fe_4(pypentO)(pym)(Oac)_2(NCS)_2(MeO)_2(H_2O)]\cdot H_2O$ (**2**). Solid lines represent the best simultaneous fit of the four sets of data with the D_{2d} symmetry model including single-ion ZFS (see text).

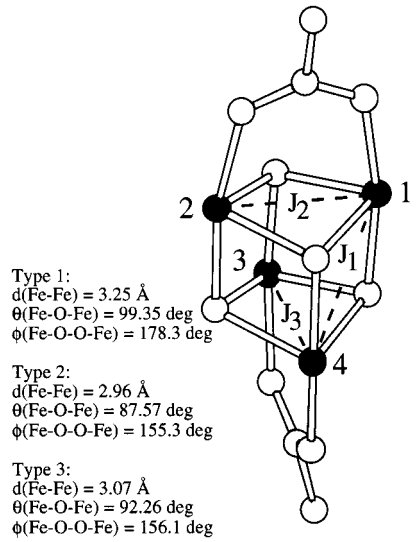

Figure 15. Schematic view of the $Fe_4O_4(Oac)_2$ core of complex **2**. Filled balls denote iron atoms, and empty ones denote bridging oxygen atoms or acetate groups. Dashed lines show the three types of Fe···Fe exchange interactions (J_1, J_2, and J_3) based on the differences in structural parameters.

cannot be compared to those obtained in this work, but the sign assignment is unquestionable. Both results confirm that the presence of an additional carboxylate bridge provides an additional exchange pathway, resulting in a bulk antiferromagnetic exchange interaction.

The temperature dependence of χT at different fields for complex **2** plotted in Figure 14 is quite similar to that for complex **1**. The temperature dependence of χT measured under a magnetic field of 1.0 T increases from a value of 14 emu K mol^{-1} at room temperature up to a maximum at 18.6 K (18.6 emu K mol^{-1}). These data were fitted using the following spin Hamiltonian:

$$\hat{H} = -2J_1(\hat{S}_1\hat{S}_3 + \hat{S}_1\hat{S}_4 + \hat{S}_2\hat{S}_3 + \hat{S}_2\hat{S}_4) - 2J_2\hat{S}_1\hat{S}_2 - 2J_3\hat{S}_3\hat{S}_4 + D(\hat{S}_{z1}^2 + \hat{S}_{z2}^2 + \hat{S}_{z3}^2 + \hat{S}_{z4}^2) \quad (2)$$

This Hamiltonian, equivalent to eq 1, differs only in some interchanges of sub-indices made to take into account the coupling scheme shown in Figure 15. With the Fe_4O_4 cubane core and the nature of bridging ligands for the different faces

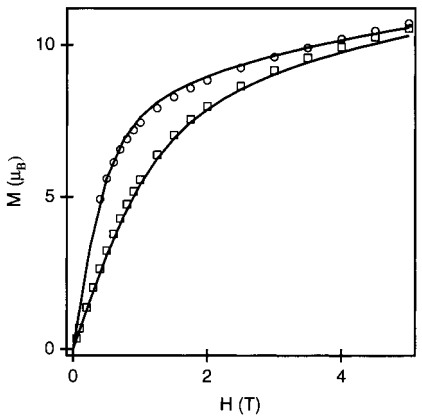

Figure 16. *M* vs *H* curves at 2 and 5 K for complex **2**. Solid lines represent the calculated curves from the best fits of $\chi_M T$ vs *T* shown in Figure 15.

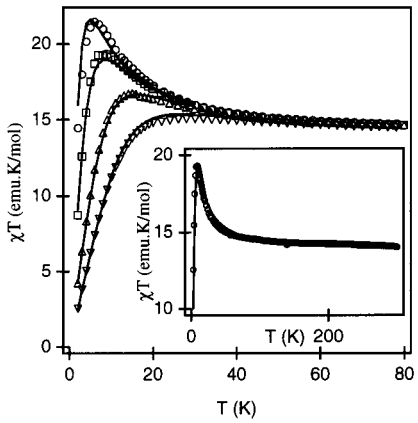

Figure 17. $\chi_M T$ product vs *T* under applied magnetic fields of 0.5, 1.0, 2.5, and 5 T for $[Fe_2(pypentO)(NCO)_3]_2$ (**3**). Solid lines represent the best simultaneous fit of the four sets of data with the symmetry model including two single-ion ZFS parameters (see text).

of the cube taken into account, it is possible to assume a D_{2d} point group symmetry. The exchange interactions J_2 and J_3 are associated with the faces including two μ_3-OR bridges and one acetate bridge, and J_1 is associated with the four other faces assumed to be equivalent. Attempts to fit with the assumption that exchange interactions corresponding to the faces involving two μ_3-OR bridges and one acetate bridge are equivalent ($J_2 = J_3$) failed: in order to obtain a good fit, these two exchange interactions must be considered independently. The best fit for the complete set of curves obtained with this assumption yielded the following set of parameters: $J_1 = 2.6\ cm^{-1}$, $J_2 = 2.5\ cm^{-1}$, $J_3 = -5.6\ cm^{-1}$, $D = 4.5\ cm^{-1}$, $g = 2.09$, and a residual $R = 1.6 \times 10^{-2}$ (solid lines in Figure 14). The low-temperature magnetization data were then satisfactorily fitted by using this set of parameters (solid lines in Figure 16). The corresponding scheme of energy levels (Figure SI-2) illustrates that the ground-state levels arise from a mixing of different spin multiplets. This result confirms the ferromagnetic nature of the interaction between irons bridged by two μ_3-OR oxygen atoms observed for complex **1**. However, this fit shows that in the case of complex **2**, the exchange interaction is ferromagnetic for one of the acetate bridged faces while it is antiferromagnetic for the other one. This result is quite surprising in view of the apparently small structural differences between the two faces.

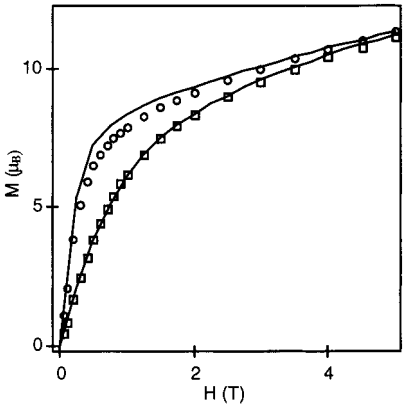

Figure 18. *M* vs *H* curves at 2 and 5 K for complex **3**. Solid lines represent the calculated curves from the best fits of $\chi_M T$ vs *T* shown in Figure 17.

The Fe−Fe distances differ only by 0.11 Å, and the most important difference is the average Fe−O−Fe angle (87.36 and 92.1° in **1** and **2**, respectively). The restricted number of iron(II)-alkoxide cubane-type structures does not allow drawing magneto-structural correlations. However, in the case of other metal centers such as nickel, differences as small as 5° in M−O−M angles induce a change in the sign of the magnetic interaction.[33]

The thermal dependence of χT for the bis-dinuclear complex **3** is plotted in Figure 17. The χT product measured under a 1.0 T magnetic field increases with decreasing temperature from 14.0 emu K mol^{-1} at 300 K up to a sharp maximum at 8 K. Below this temperature, the χT product decreases very sharply due to the splitting of the ground state. The thermal variation of χT presents an important dependence to the magnetic field, and at 5 *T*, the sharp maximum has disappeared. With the symmetry of complex **3** taken into account, the temperature dependence of χT was fitted using the following Hamiltonian:

$$\hat{H} = -2J_1(\hat{S}_1\hat{S}_2 + \hat{S}_3\hat{S}_4) - 2J_2\hat{S}_1\hat{S}_3 + D(\hat{S}_{z2}^2 + \hat{S}_{z4}^2) + D'(\hat{S}_{z1}^2 + \hat{S}_{z3}^2) \quad (3)$$

J_1 corresponds to the intradinuclear interactions and J_2 to the interdinuclear one (for the purpose of using eq 3 for both **3** and **4**, the spin states S_3 and S_4 in complex **3** are assigned to Fe1′ and Fe2′, respectively); *D* corresponds to the pentacoordinated site and *D*′ to the octahedral one. Attempts to fit with $D = D'$ failed, and the only possibility was to associate a different zero-field splitting parameter to each type of iron site. The best fit obtained by taking into account parallel and perpendicular susceptibilities yielded positive values for the single-ion anisotropy parameters ($J_1 = 0.6\ cm^{-1}$, $J_2 = 0.7\ cm^{-1}$, $D = 12.1\ cm^{-1}$, $D' = 4.2\ cm^{-1}$, $g = 2.14$, and a residual $R = 3.4 \times 10^{-2}$). However, the low-temperature magnetization data (Figure 18) could not be satisfactorily simulated with this set of parameters. Therefore, a simultaneous fit of the χT data at different fields through integration over all orientations of the axis of anisotropy with respect to the magnetic field was performed. The best fit (solid lines in Figure 17) yielded the following set of parameters, including negative zero-field splitting param-

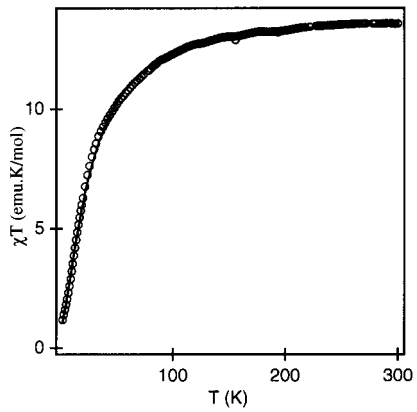

Figure 19. $\chi_M T$ product vs T under an applied magnetic field of 1.0 T for $[Fe_2(pypentO)(N_3)_3]_2$ (**4**). Solid lines represent the best fit of the data with the symmetry model including two single-ion ZFS parameters (see text).

eters: $J_1 = 0.25$ cm^{-1}, $J_2 = 1.2$ cm^{-1}, $D = -5.6$ cm^{-1}, $D' = -4.5$ cm^{-1}, $g = 2.14$, and a residual $R = 4.7 \times 10^{-2}$. This is in agreement with the interpretation of the Mössbauer spectra obtained in applied magnetic fields that indicates that both iron sites are characterized by negative ZFS terms (-4 to -7 cm^{-1}). Additional support to this result arises from the good fit of the low-temperature magnetization data obtained by using this set of parameters (solid lines in Figure 18). The 2 K magnetization data evidence a change in slope: at low magnetic field, the parallel contribution prevails due to a quick saturation of the high spin value of the ground state and the slope is steep. At a higher magnetic field, where the parallel contribution is saturated, the effect of the perpendicular contribution prevails: due to the small splitting produced by a perpendicular field, the slope is gradual up to saturation. In the case of complex **3**, due to the high spin value ($M = \pm 8$) these effects are very clear at low temperature. Of course, in the case of an $M = 0$ ground state and positive ZFS parameters, the shape of the magnetization curve would be very different. The scheme of energy levels for this complex (Figure SI-3) presents an unusual structure due to the interpenetration of several ZFS split multiplets with the $\pm S$ doublet ground state: the three ferromagnetic interactions ensure a maximum contribution to the $S_T = 8$ ground state, but this state is largely mixed with the first excited doublet states with quantum numbers ± 4 and 0 due to the small values of J_1 and J_2 with respect to D and D'. Inclusion of the rhombic terms $E(S_{x1}^2 - S_{y1}^2 + S_{x4}^2 - S_{y4}^2) + E'(S_{x2}^2 - S_{y2}^2 + S_{x3}^2 - S_{y3}^2)$ would lift the degeneracy of the energy levels with $M \neq 0$. From the magnetic Mössbauer spectra at 4.2 K, the splitting of the two ground state levels was estimated to be small but nonzero. Such a splitting, however, would not critically affect the conclusions drawn from the measurements shown in Figure 18, i.e., with the fit parameters used for Figures 18 and SI-3 and $E/D = 0.33$ (see caption to Figure 9) the degeneracy of energy levels with $M \neq 0$ would be lifted by 0.02 cm^{-1}.

The thermal dependence of χT for the bis-dinuclear complex **4** is plotted in Figure 19. The χT product measured under a 0.9 T magnetic field decreases continuously with decreasing temperature from 13.2 emu K mol^{-1} at 300 K toward zero at low temperature. Assuming that the exchange pathway symmetry is similar to that in complex **3**, the Hamiltonian of eq 3 has been used in order to fit the magnetic data. The best fit was obtained for the following set of parameters: $J_1 = -1.2$ cm^{-1}, $J_2 = -2.2$ cm^{-1}, $D = 7.8$ cm^{-1}, $D' = 2.5$ cm^{-1}, $g = 2.20$, paramagnetic impurity = 6.1%, and a residual $R = 1.51 \times 10^{-2}$. Complex **4** is the first example of an azido-bridged discrete polynuclear ferrous compound. This tetranuclear iron(II) structure results from the bridging of two $Fe_2(pypentO)(N_3)_2$ dinuclear moieties through two end-on azido anions. This type of exchange pathway would be expected to yield a ferromagnetic J_2 interaction as observed for complex **3** and for end-on azido-bridged copper(II),[40] nickel(II),[4] Co(III),[41] and Fe(III)[42] discrete polynuclear complexes. Each constituting $Fe_2(pypentO)(N_3)_2$ unit results from the bridging of two iron(II) through one end-on azido anion and the central O_{alkoxo} of the pentadentate pypentO$^-$ ligand. There is no example of mixed end-on azido and O_{alkoxo} bridges in the literature, and by comparison with complex **3** (mixed μ_2-N-cyanato and O_{alkoxo} bridges), this type of exchange pathway would be expected to yield a weaker ferromagnetic J_1 interaction. Consequently, the whole space of parameters has been scanned in order to check for other possible minima when one of the two exchange parameters is ferromagnetic. (Due to the absence of a maximum in the experimental χT product, it is clear that both exchange interactions cannot be ferromagnetic.) Two other minima have been obtained, one for each of the two ferromagnetic−antiferromagnetic combinations. When J_1 (exchange through O_{alkoxo} and end-on N_{azido} bridges) is ferromagnetic, the ZFS parameter D (pentacoordinated sites) is abnormally high (21.4 cm^{-1}) and the fit is poor ($R = 4.9 \times 10^{-2}$). However, when J_2 (exchange through two end-on N_{azido}) is ferromagnetic, the ZFS parameter D has a reasonable value and the quality of the fit is better ($J_1 = -2.6$ cm^{-1}, $J_2 = 0.75$ cm^{-1}, $D = 6.3$ cm^{-1}, $D' = 1.6$ cm^{-1}, $g = 2.18$, paramagnetic = impurity 5.8%, and $R = 2.8 \times 10^{-2}$, solid line in Figure 19). In this complex, due to the antiferromagnetic nature of the ground state, the magnetization data do not yield additional information supporting one of the solutions. The fits in the case of complex **4** are not sensitive to the sign of D: due to the antiferromagnetic interaction, the ground state is not magnetic and D contributes only to higher energy states; its influence is weak due to simultaneous thermal population of several excited levels very close in energy. Consequently, although the best fits are obtained with positive D values, the structural similarity between complexes **3** and **4** suggests that the possibility of negative D values should not be excluded. The full schemes of energy levels obtained from both sets of fitting parameters with either positive (Figure SI-4) or negative (Figure SI-5) D and D' values are very similar and show an interpenetration of zero-field split spin manifolds,

(40) Maji, T. K.; Mukherjee, P. S.; Koner, S.; Mostafa, G.; Tuchagues, J.-P.; Chaudhuri, N. R. *Inorg. Chim. Acta* **2001**, *314*, 111 and refs therein.
(41) Drew, M. G. B.; Harding, C. J.; Nelson, J. *Inorg. Chim. Acta* **1996**, *246*, 73.
(42) Reddy, K. R.; Rajasekharan, M. V.; Tuchagues, J.-P. *Inorg. Chem.* **1998**, *37*, 5978.

lending support to the above considerations on the signs of *J*s and *D*s for complex **4**.

Conclusions

This study shows the variety of molecular architectures that may be obtained from the flexible pentadentate pypentO ligand. Small changes such as the nature of the pseudo-halide anion or the reaction conditions yield dramatic changes in the iron(II)-alkoxide chemistry. The detailed study of magnetic and Mössbauer properties for the two $[Fe_4O_4]$ cubane-like cores of **1** and **2** and the two Fe_4 linear cores including O_{alkoxo} and $N_{cyanato}$ (**3**) or N_{azido} (**4**) bridges shows how minor structural differences may induce significant changes in the electronic structure of the metal cores of these unprecedented tetranuclear ferrous complexes including bridging or terminally coordinated pseudo-halides.

Acknowledgment. We thank Dr. Simopoulos for assistance with the magnetic field Mössbauer measurements. Y.S. thanks Dr. Petrouleas for support. The European Community is acknowledged for support through a postdoctoral grant to J.M.C.J. within the framework of the TMR contract FMRX- CT980174.

Supporting Information Available: Mössbauer parameters obtained from fitting the 13 spectra (30−270 K) of complex **1** (Table SI-1), schemes of energy levels obtained from the best fits of magnetic susceptibility data for compounds **1**−**4** (Figures SI-1−SI-5), X-ray crystallographic files of $[Fe_4(pypentO)(pym)_3(Oac)(NCS)_3]\cdot 1.5EtOH$ (**1**), $[Fe_4(pypentO)(pym)(Oac)_2(NCS)_2(MeO)_2(H_2O)]\cdot H_2O$ (**2**), and $[Fe_2(pypentO)(NCO)_3]_2$ (**3**), and $[Fe_2(pypentO)(N_3)_3]_2$ (**4**) in CIF format. This material is available free of charge via the Internet at http://pubs.acs.org.

IC010787+